Pathway toward Large Two-Dimensional Hexagonally Patterned Colloidal Nanosheets in Solution

Bo Ni,[†] Mingjun Huang,[†] Ziran Chen,[†] Yingchao Chen,[§] Chih-Hao Hsu,[†] Yiwen Li,[†] Darrin Pochan,[§] Wen-Bin Zhang,*[,†,‡] Stephen Z. D. Cheng,*[,†] and Xue-Hui Dong*[,†]

[†]Department of Polymer Science, The University of Akron, Akron, Ohio 44325-3909, United States
[‡]Key Laboratory of Polymer Chemistry and Physics of the Ministry of Education, College of Chemistry and Molecular Engineering, Center for Soft Matter Science and Engineering, Peking University, Beijing 100871, P. R. China
[§]Department of Materials Science & Engineering, University of Delaware, Newark, Delaware 19716, United States
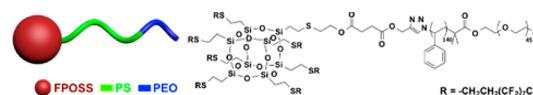
Ⓢ *Supporting Information*

ABSTRACT: We report the solution self-assembly of an ABC block terpolymer consisting of a polystyrene-*block*-poly(ethylene oxide) (PS-*b*-PEO) diblock copolymer tail tethered to a fluorinated polyhedral oligomeric silsesquioxane (FPOSS) cage in 1,4-dioxane/water. With increasing water content, abundant unconventional morphologies, including circular cylinders, two-dimensional hexagonally patterned colloidal nanosheets, and laterally patterned vesicles, are sequentially observed. The formation of toroids is dominated by two competing free energies: the end-cap energy of cylinders and the bending energy to form the circular structures. Incorporating the super-hydrophobic FPOSS cages enhances the end-cap energy and promotes toroid formation. Lateral aggregation and fusion of the cylinders results in primitive nanosheets that are stabilized by the thicker rims to partially release the rim-cap energy. Rearrangement of the parallel-aligned FPOSS cylindrical cores generates hexagonally patterned nanosheets. Further increasing the water content induces the formation of vesicles with nanopatterned walls.

Nature creates self-organized, complex hierarchical structures with biomolecules as the foundation of delicate life. The past several decades have witnessed great efforts to mimic these sophisticated structures using synthetic approaches.[1] One of the most significant developments is the recognition of the ability of amphiphilic block copolymers to form ordered structures at the nanometer scale, leading to various applications in emerging nanotechnologies.[2] Self-assembly of diblock copolymers in solution has been well-documented.[3] The selective partitioning of amphiphilic blocks results in three representative equilibrium morphologies: spheres, cylinders, and vesicles.[3b] Vesicles are essentially closed bilayer sheets. These 2D bilayer sheets are not only scientifically intriguing but also technologically relevant. They bridge cylindrical and vesicular morphologies and constitute important intermediate stages during the structural transitions.[4] Furthermore, these ordered two-dimensional (2D) nanostructures, especially with large size, are technologically important for pattern transformation in nanolithography applications. They are, however, hardly seized because of the existence of lateral surfaces with high surface free energy.[4] To date there are only a few examples of 2D nanostructured sheets made from amphiphilic block copolymers and other designed conjugates in solution.[5] The small size and lack of hierarchical structures limit their potential applications. Li et al.[5c] reported the first example of 2D nanosheets with hexagonal-packed subdomains using miktoarm star terpolymers. A complete understanding of the formation of this unprecedented structure is, however, still some distance away.

We recently designed and synthesized a series of block polymers consisting of a functionalized molecular nanoparticle and linear polymer.[6] The significant topological deviations from traditional coil—coil block copolymers result in unique features in their self-assembly.[7] The geometric constraints of the molecular nanoparticles enhance the immiscibility compared with their linear counterparts.[6] Herein we report the micellization of a specifically designed ABC block terpolymer with a fluorinated polyhedral oligomeric silsesquioxane (FPOSS) head and a polystyrene-*block*-poly(ethylene oxide) (PS-*b*-PEO) tail (FPOSS-PS$_{140}$-*b*-PEO$_{45}$, where the subscripts refer to the degree of polymerization; Chart 1). The syntheses are described

Chart 1. Schematic Illustration and Chemical Structure of the ABC Block Terpolymer

in Scheme S1 and Figures S1 and S2 in the Supporting Information (SI).[8] The polymer was dissolved in 1,4-dioxane (0.5 wt %) as a stock solution. To induce micelle formation, deionized water was slowly added to 2.0 g of stock solution at an average rate of 20 mg/h. We found that in addition to forming regular spherical and cylindrical micelles, this terpolymer is able to construct various unconventional, metastable micellar morphologies. The appearance of these unusual micellar morphologies provides a unique opportunity to investigate the pathway from one equilibrium micelle to another. Particularly, we are interested in arresting large 2D hexagonally patterned colloidal nanosheets before the system enters the vesicle region.

At low water contents, spheres and cylinders can be observed. They are similar to those from amphiphilic diblock polymers, yet nanophase separation between the FPOSS and PS blocks in the hydrophobic core also occurs.[9] Spherical micelles form at a water content of 10% with a uniform size distribution, as characterized by transmission electron microscopy (TEM) (Figure S3a) and dynamic light scattering (DLS) (Figure S4), which gave average diameters of 27 and ~60 nm, respectively. The difference originates from the fact that DLS characterizes the hydrodynamic size while TEM is sensitive only to the dense, hydrophobic core.[10] A core−shell−corona structure can be anticipated as the center part of the spheres is darker than the peripheral area (Figure S3a). Considering that water is a good solvent for PEO blocks, a poor solvent for PS blocks, and an extremely poor solvent for FPOSS cages, these FPOSS cages must first aggregate to form the inner core surrounded by the PS shell. The micelle is further stabilized by the PEO corona. Because of the asymmetric volume fraction of the PS blocks and FPOSS cages in the hydrophobic core ($f_{PS} = 0.86$; see the SI), a curved interface is preferred. This molecular arrangement is consistent with the TEM images, since FPOSS cages possess a higher electron density than PS blocks.[11] The spheres transform into wormlike cylinders when the water content reaches 18%. The average diameter is 28 nm (Figure S3b). A dark line at the center of each cylinder along the long axis can be identified, indicating that the cylinders also adopt the core−shell−corona arrangement (see the model in Figure S3b).

Circular cylinders can be observed at water contents of 22−34%, including toroids (Figure 1a), tadpoles and dumbbells
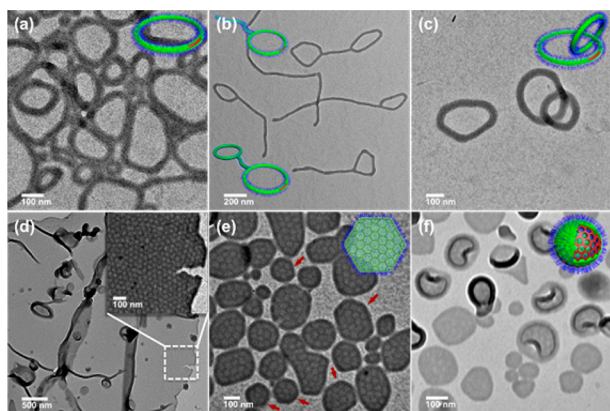

Figure 1. TEM images of (a) toroids, (b) tadpoles and dumbbells, (c) interlocked toroids, (d, e) 2D nanosheets, and (f) laterally structured vesicles. FPOSS, red; PS, green; PEO, blue.

(Figure 1b), interlocked toroids (Figure 1c), etc. Among them, the toroid is the most prevalent morphology. These toroidal structures have a similar diameter and identical core−shell−corona molecular arraignment as the cylinders and thus must originate from closure of cylinders as the water content increases.[12] No toroids were observed in control experiments with the diblock copolymer precursor (PS_{140}-b-PEO_{45}) under the same experimental conditions. The incorporation of FPOSS cages is thus the determining factor in the formation of these circular micelles.

We first investigate the closure of cylinders on the basis of equilibrium thermodynamics.[3b,13] There are three major contributions to the overall free energy (F) that regulate the equilibrium micellar morphologies: intercorona interactions due to repulsion among hydrophilic blocks (F_{corona}); interfacial energy between the hydrophobic core and the solvent ($F_{interface}$); and stretching of hydrophobic blocks within the core (F_{core}):[3b]

$$F = F_{corona} + F_{interface} + F_{core} \qquad (1)$$

For cylinders, eq 1 is valid only in the ideal case that the micelles have infinite length, in which the ends can be ignored. In reality, an additional term associated with end caps ($F_{end\text{-}caps}$) should also be included:

$$F_{cylinders} = F_{corona} + F_{interface} + F_{core} + 2F_{end\text{-}caps} \qquad (2)$$

It should be noted that in our case there are always two interfaces, one between the PS block and the surrounding solvent and one between the PS blocks and FPOSS cages. As the free energy of latter interaction is constant, the term $F_{interface}$ in eq 2 specifically refers to the interfacial energy between the PS shell of the cylindrical body and the solvent. The coefficient of 2 for $F_{end\text{-}caps}$ is included because each cylinder has two approximately hemispherical end caps. These end caps have unfavorably high energy, providing the driving force for continuous growth of cylinders. The block copolymers residing within the end-caps are subjected to spherical packing, while those in the main body experience cylindrical packing.[14] The interfacial area per molecule, s, strongly depends on the micellar geometry (eq S1 in the SI).[3b,15] To maintain an identical value of s, the radius of the end-cap hemispheres should be larger than the radius of the cylindrical body by a factor of $^3/_2$.[14] However, in our experimental observations (as in most experimental observations) the end caps and body of the cylindrical micelles have identical sizes. The s of the end caps must thus increase to accommodate this arrangement, which results in molecular packing frustration and leads to an increase in interfacial energy.[14] The end-cap energy can be calculated using the opposing forces model (eqs S2 and S3), which gives ~$140k_BT$ per cylinder (Table S1 in the SI).[4,14−16] This term should be higher in our case because the superhydrophobic FPOSS core increases the surface tension of the cylindrical end caps.

The formation of toroids eliminates these end caps at the expense of an energetic penalty associated with bending ($F_{bending}$) and a loss of configurational entropy ($F_{entropy}$) (eq 3):

$$F_{toroids} = F_{corona} + F_{interface} + F_{core} + F_{bending} + F_{entropy} \qquad (3)$$

For a toroid with a radius of 100 nm, the bending energy of a uniform cylinder (eq S4)[14] is estimated to be $20k_BT$ per micelle (Table S1). The free energy penalty associated with the loss of configurational entropy ($F_{entropy}$) can be estimated using a random walk model in a 3D cubic lattice (eq S5)[14] and is typically around $2−5k_BT$ (Table S1).

Comparison of eqs 2 and 3 shows that the energies due to bending and entropy loss during ring closure are insignificant relative to the cylinder end-cap energy (Table S1). The formation of toroids is thus energetically favorable, with a free energy decrease on the order of $100k_BT$ per cylinder assuming that F_{corona}, $F_{interface}$, and F_{core} are identical in both of the cases.[12c] On the other hand, the closure process is generally recognized to be kinetically less favorable, which makes the toroidal morphology hard to capture.[12c] Theoretical studies indicate that a toroid-prevalent regime could exist if the end-cap energy is high enough.[14,17] Incorporation of the FPOSS cages increases the end-cap energy, making the toroid a dominating morphology.

The tadpoles and dumbbells can be considered as toroid-end-capped cylinders (Figure 1b). There are two possible fusion

pathways: one end of a cylinder attaches to a pre-existing toroid (intermicellar), or "bites" itself at an internal location on the cylinder body (intramicellar). They are thermodynamically identical in terms of the final free energy that a Y-shaped junction forms, providing alternative ways to remove energetically unfavorable end caps. If intermicellar fusion is dominant, other types of structures such as multiple cylinders attached to one toroid should also be generated. However, the observed topologies are almost exclusively single cylindrical tail/linkage, indicating that the self-biting pathway may be dominant in our case since the micellar solution is very dilute. The interlocked toroids (Figure 1c) represent a circumstance in which two neighboring toroids thread each other during their ring closures, though the probability of the formation of this topology is typically rather small.

The most intriguing micellar morphology, 2D hexagonally patterned nanosheets, is observed when the water content reaches 41% (Figure 1d,e). Under mild stirring, the size of these sheets can reach tens of micrometers (Figure 1d). These nanosheets possess hexagonally patterned internal structures (Figure 1d inset). The dark and gray domains can be assigned to the FPOSS cages and PS blocks, respectively, on the basis of their electron densities.[11] With vigorous stirring, the strong shear force interrupts the growth of large sheets, resulting in small debris with sizes typically below 1 μm that tend to have faceted or hexagonal shapes (Figure 1e, indicated by the arrows). These two different-sized nanosheets possess identical structures and follow the same formation mechanisms. AFM images of these nanosheets reveal that they have a thicker boundary of 21 nm (Figure S5) compared with that of the interior (18 nm). The thickness difference is also confirmed in the TEM images by the appearance of darker edges (Figure 1d,e). These 2D nanosheets are 2D layers with hexagonally connected FPOSS domains embedded inside a continuous PS matrix that is further covered by the PEO corona (see the proposed model in Figure 1e).

The formation of these nanosheets involves three steps, as captured by TEM images: (i) lateral aggregation of cylindrical micelles into 2D bundles (Figure 2a); (ii) fusion of the
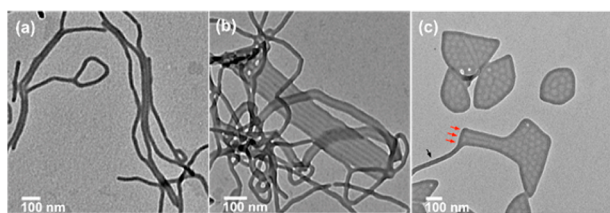

Figure 2. Intermediate states during the formation of nanosheets: (a) aggregation; (b) fusion; (c) rearrangement.

neighboring PS shells to form primitive nanosheets (Figure 2b); and (iii) rearrangment of the FPOSS cylindrical cores into hexagonally connected networks (Figure 2c). The pathway is also schematically illustrated in Figure 3. The aggregation occurs when the water content reaches 34%, among approaching free cylinders (Figures 2a and S6), between cylinders and toroids (Figure S7a), within toroids (Figures S7b,c), etc. The aggregation develops in two dimensions to avoid trapping of the PEO blocks in the hydrophobic core. With further addition of water (41%), the PS shells fuse to form a continuous matrix with a wavelike surface profile (Figure S8). The spacing between neighboring FPOSS cylindrical cores within the nanosheets is around 35 nm (Figure 2c), which is larger than the diameter of

the free cylinders (28 nm). The FPOSS cylindrical cores in these primitive nanosheets continuously rearrange under the same water content (41%). This rearrangement process starts from the emergence of "bridges" between neighboring FPOSS cores where the coverage by PS blocks is relatively less dense (Figure S8). This results in ladderlike networks (Figure S9), which are randomly arranged at the early stage. With increasing packing order, the honeycomb-like network is finally formed. The intermediate states are confirmed by cryo-TEM images (Figure S10), which provide in situ morphological information in solution. The rearrangement occurs as soon as the primitive nanosheets form, and thus, the overall pathway is in an overlapped sequence. The resultant nanosheets further grow via mutual amalgamation and/or incorporation of free cylindrical micelles (or cylindrical tails emanating from the primitive nanosheets) (Figure S11). This is evidenced by the nanosheets with parallel-aligned FPOSS cores at the peripheries, while a perfect honeycomb-like structure has already formed at the inner region (Figure S12). These nanosheets gradually approach a faceted hexagonal shape, as determined by the internal structure, and reach the minimum surface tension.

The pathway shown in Figure 3 is driven by stepwise free energy minimization. Fusion of the individual cylinders (Figure
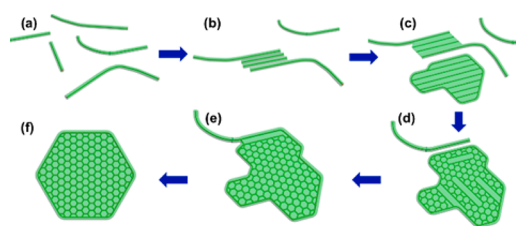

Figure 3. Schematic illustration of the formation pathway of 2D nanosheets. PEO has been omitted for clarity.

3a−c) occurs because the short PEO corona cannot provide sufficient steric repulsion (F_{corona}) to balance the excess interfacial energy ($F_{interface}$) with increasing water content, while the rearrangement of FPOSS cylindrical cores (Figure 3c,d) is driven by release of the stretching of the PS blocks. This can be illustrated by examining the overall free energy of micelles (eq 1). The contributions of F_{core}, $F_{interface}$, and F_{corona} to the overall free energy were calculated and are shown in Table S2. It is evident that individual cylinders and parallel-aligned nanosheets possess similar overall free energies ($10.6k_BT$ vs $10.9k_BT$ per molecule) at the transition stage (Figure 3b). As the water content increases further, $F_{interface}$ gradually becomes dominant. The cylinders tend to shrink their interfacial area by rearranging the molecular packing of the block copolymer in micelles from cylindrical ($F_{interface} = 7.4k_BT$ per molecule) to lamellar ($F_{interface} = 3.7k_BT$ per molecule) to reduce the corresponding interfacial energy (eq S1) at the expense of stretching of the PS blocks to fit the increasing spacing between neighboring FPOSS cores ($F_{core} = 0.98k_BT$ for cylinders vs $3.31k_BT$ for nanosheets) and steric repulsion between the PEO coronas ($F_{corona} = 2.22k_BT$ for cylinders vs $3.94k_BT$ for nanosheets). Beyond the crossover region (Figure 3b), the free energy decrease due to the reduction in interfacial area exceeds the energy penalty from chain stretching and repulsion, and fusion is thus energetically favorable. The transition from parallel-aligned nanosheets (Figure 3c) to hexagonally patterned nanosheets (Figure 3d), on the other hand, is driven by the release of chain stretching of the PS blocks. The latter has a much higher PS chain number

density, which leads to local overcrowding in the honeycomb chambers and recovers most of the stretched PS blocks (see Figure S5).

The stability of nanosheets depends on two competing free energies: the rim-cap energy ($F_{rim-cap}$), which like the end-cap energy of cylinders originates from molecular packing frustration at the lateral interfaces, and the bending energy ($F_{bending}$), which describes the energy penalty for deviation from the spontaneous curvature.[4] The bending energy is independent of the size of the vesicle and equal to $F_{bending} = 8\pi\kappa_c$, where κ_c is the bending modulus.[4,15,18] A typical value of $3800\pi k_B T$ per micelle is required to bend block-copolymer lamellae into a spherical vesicle (see the SI).[18] Considering the incorporation of the FPOSS cages, the bending modulus, and thus the bending energy, should be larger than the estimation.

Following a similar argument as in the case of cylinders, the interfacial area per molecule in the rim is larger than in the interior, which leads to excess surface energy.[14,19] As a first approximation, the rim-cap energy is estimated to be $\sim4200\pi k_B T$ per micelle for a nanosheet with a diameter of 600 nm (see the SI).[19] The excess lateral free energy makes nanosheets prone to close up to form vesicles. In our case, the rim of the nanosheet has a larger diameter than the interior lamellar region, which partially releases the packing frustration ($\sim3400\pi k_B T$; see the SI) to the extent that the rim-cap energy is no longer dominant. The nanosheets are thus stabilized and experimentally accessible.

Vesicles eventually form when the water content exceeds 55% (Figure 1f). They have a hexagonal pattern on the micellar walls and thus must originate from the nanosheets. The rim-cap energy of nanosheets becomes dominant with increasing water content, which eventually induces their closure. The vesicles coexist with nanosheets that are too small to form closed structures.[4]

In summary, a variety of unconventional morphologies are observed in solution with a FPOSS-based terpolymer. At low water contents, spheres and cylinders with the core—shell—corona structure are formed. The high surface tension of the end caps drives the formation of circular cylinders. The 2D hexagonally patterned nanosheets are stabilized by thick rims that partially release the excess rim-cap energy. Vesicles with hexagonally patterned walls eventually form as the water content is further increased. This study not only exhibits abundant unique morphologies but also promotes fundamental understanding of the pathways for transformations between different morphologies in solution.

ASSOCIATED CONTENT

Ⓢ Supporting Information

Supplementary characterizations. This material is available free of charge via the Internet at http://pubs.acs.org.

AUTHOR INFORMATION

Corresponding Authors
*xd4@zips.uakron.edu
*scheng@uakron.edu
*wenbin@pku.edu.cn

Notes
The authors declare no competing financial interest.

ACKNOWLEDGMENTS

REFERENCES

(1) Whitesides, G. M.; Grzybowski, B. *Science* **2002**, *295*, 2418.

(2) (a) Park, M. *Science* **1997**, *276*, 1401. (b) Savic, R.; Luo, L.; Eisenberg, A.; Maysinger, D. *Science* **2003**, *300*, 615.

(3) (a) Price, C. In *Developments in Block Copolymers*; Goodman, I., Ed.; Applied Science: London, 1982. (b) Zhang, L.; Eisenberg, A. *Polym. Adv. Technol.* **1998**, *9*, 677. (c) Hamley, I. W. *The Physics of Block Copolymers*; Oxford University Press: Oxford, U.K., 1998. (d) Riess, G. *Prog. Polym. Sci.* **2003**, *28*, 1107. (e) Zhulina, E. B.; Adam, M.; LaRue, I.; Sheiko, S. S.; Rubinstein, M. *Macromolecules* **2005**, *38*, 5330. (f) Mai, Y.; Eisenberg, A. *Chem. Soc. Rev.* **2012**, *41*, 5969.

(4) Antonietti, M.; Forster, S. *Adv. Mater.* **2003**, *15*, 1323.

(5) (a) Li, Z.; Chen, Z.; Cui, H.; Hales, K.; Qi, K.; Wooley, K. L.; Pochan, D. J. *Langmuir* **2005**, *21*, 7533. (b) Edmonds, W. F.; Li, Z.; Hillmyer, M. A.; Lodge, T. P. *Macromolecules* **2006**, *39*, 4526. (c) Li, Z.; Hillmyer, M. A.; Lodge, T. P. *Nano Lett.* **2006**, *6*, 1245. (d) Zhou, Z.; Li, Z.; Ren, Y.; Hillmyer, M. A.; Lodge, T. P. *J. Am. Chem. Soc.* **2003**, *125*, 10182.

(6) (a) Yu, X.; Li, Y.; Dong, X.-H.; Yue, K.; Lin, Z.; Feng, X.; Huang, M.; Zhang, W.-B.; Cheng, S. Z. D. *J. Polym. Sci., Part B: Polym. Phys.* **2014**, *52*, 1309. (b) Zhang, W.-B.; Yu, X.; Wang, C.-L.; Sun, H.-J.; Hsieh, I.-F.; Li, Y.; Dong, X.-H.; Yue, K.; Horn, R. V.; Cheng, S. Z. D. *Macromolecules* **2014**, *47*, 1221.

(7) (a) Yu, X.; Zhong, S.; Li, X.; Tu, Y.; Yang, S.; Horn, R. M. V.; Ni, C.; Pochan, D. J.; Quirk, R. P.; Wesdemiotis, C.; Zhang, W.-B.; Cheng, S. Z. D. *J. Am. Chem. Soc.* **2010**, *132*, 16741. (b) Yu, X.; Zhang, W. B.; Yue, K.; Li, X.; Liu, H.; Xin, Y.; Wang, C. L.; Wesdemiotis, C.; Cheng, S. Z. *J. Am. Chem. Soc.* **2012**, *134*, 7780. (c) Yu, X.; Yue, K.; Hsieh, I. F.; Li, Y.; Dong, X. H.; Liu, C.; Xin, Y.; Wang, H. F.; Shi, A. C.; Newkome, G. R.; Ho, R. M.; Chen, E. Q.; Zhang, W. B.; Cheng, S. Z. *Proc. Natl. Acad. Sci. U.S.A.* **2013**, *110*, 10078.

(8) Ni, B.; Dong, X.-H.; Chen, Z.; Lin, Z.; Li, Y.; Huang, M.; Fu, Q.; Cheng, S. Z. D.; Zhang, W.-B. *Polym. Chem.* **2014**, *5*, 3588.

(9) (a) Li, Z.; Kesselman, E.; Talmon, Y.; Hillmyer, M. A.; Lodge, T. P. *Science* **2004**, *306*, 98. (b) Moughton, A. O.; Hillmyer, M. A.; Lodge, T. P. *Macromolecules* **2012**, *45*, 2.

(10) Yuan, X.; Jiang, M.; Zhao, H.; Wang, M.; Zhao, Y.; Wu, C. *Langmuir* **2001**, *17*, 6122.

(11) Mabry, J. M.; Vij, A.; Iacono, S. T.; Viers, B. D. *Angew. Chem., Int. Ed.* **2008**, *47*, 4137.

(12) (a) Jain, S.; Bates, F. S. *Science* **2003**, *300*, 460. (b) Pochan, D. J.; Chen, Z.; Cui, H.; Hales, K.; Qi, K.; Wooley, K. L. *Science* **2004**, *306*, 94. (c) Cui, H.; Chen, Z.; Wooley, K. L.; Pochan, D. J. *Soft Matter* **2009**, *5*, 1269. (d) Huang, H.; Chung, B.; Jung, J.; Park, H. W.; Chang, T. *Angew. Chem., Int. Ed.* **2009**, *48*, 4594. (e) Chen, Z.; Cui, H.; Hales, K.; Li, Z.; Qi, K.; Pochan, D. J.; Wooley, K. L. *J. Am. Chem. Soc.* **2005**, *127*, 8592.

(13) Zhulina, E. B.; Borisov, O. V. *Macromolecules* **2012**, *45*, 4429.

(14) May, S.; Ben-Shaul, A. In *Giant Micelles: Properties and Applications*; Zana, R., Kaler, E., Eds.; CRC Press: Boca Raton, FL, 2007.

(15) Bhargava, P.; Zheng, J. X.; Li, P.; Quirk, R. P.; Harris, F. W.; Cheng, S. Z. D. *Macromolecules* **2006**, *39*, 4880.

(16) (a) Israelachvili, J. *Intermolecular and Surface Forces*; Academic Press: Waltham, MA, 1992. (b) May, S.; Ben-Shaul, A. *J. Phys. Chem. B* **2001**, *105*, 630.

(17) van der Schoot, P.; Wittmer, J. P. *Macromol. Theory Simul.* **1999**, *8*, 428.

(18) Bermudez, H.; Hammer, D.; Discher, D. *Langmuir* **2004**, *20*, 540.

(19) May, S. *Eur. Phys. J. E* **2000**, *3*, 37.